Co-synthesis of ZnO–CuO Nanostructures by Directly Heating Brass in Air**

By *Yanwu Zhu, Chorng-Haur Sow,* Ting Yu, Qing Zhao, Pinghui Li, Zexiang Shen, Dapeng Yu*, and *John Thiam-Leong Thong*

ZnO–CuO nanostructures have been simultaneously synthesized by directly heating a CuZn alloy (brass) on a hotplate in ambient conditions. Depending on the Zn concentrations in the brasses, the dominant products transition from CuO nanowires to ZnO nanostructures. By changing the growth temperature and local Zn contents, 1D ZnO nanowires/nanoflakes, 2D ZnO nanosheets, and complicated 3D ZnO networks are obtained. Electron microscopy studies show that the as-synthesized ZnO nanoflakes and nanosheets are single crystalline. Based on "self-catalytic" growth, a tip-growth mechanism for ZnO nanostructures is discussed, in which the Cu in brass plays an important role to confine the lateral growth of ZnO. Finally, the electron field emission from the ZnO–CuO hybrid systems is tested for the demonstration of potential applications.

1. Introduction

1D nanomaterials have attracted much attention due to their unique properties.[1] With a wide bandgap of 3.37 eV and a large exciton energy of 60 meV, ZnO nanostructures have attracted much research interest for their potential applications in UV lasers,[2] field emitters,[3,4] sensors,[5] catalysts,[6] solar cells,[7] hydrogen-storage devices,[8] and field-effect transistors.[9] Recently, a variety of ZnO nanostructures, including nanowires,[2–5,8,9] nanotubes,[10] nanobelts,[11] nanoneedles,[6] nanorings,[12] nanocombs,[13] nanosheets,[7] nanowalls,[14] tetrapods,[15] and hierarchical[16] and complex nanostructures,[17] have been demonstrated and well documented. Such a rich family of ZnO nanostructures provides numerous opportunities for researchers to explore their properties and potential applications. For the synthesis of ZnO nanostructures, many

different approaches have been developed, such as chemical vapor deposition,[2,3,6,9] thermal evaporation,[5,8,11–13,15] template methods,[18] pulsed-laser deposition,[19] and solution-phase deposition.[4,7,10,17] Recently, the syntheses of ZnO nanowires[20,21] and nanobelts[22,23] have been achieved by directly oxidizing Zn metals in appropriate oxygen atmospheres in tube furnaces. With this method, the morphology of products is controlled mainly by the growth temperature, oxygen partial pressure, and flow rate of the carrier gas.[21–23]

Another simpler alternative is to directly oxidize metals in air. Such a synthesis can be carried out on a hotplate without any flow rate or pressure control. Moreover, the chamber-free approach is suitable for mass production for future large-scale applications. This cost-effective and efficient method has been proven to be successful in the fabrication of CuO nanowires,[24] Co_3O_4 nanowalls,[25] Fe_2O_3 nanoflakes,[26,27] and nanowalls.[28] However, due to the low melting point and high vapor pressure of Zn, control of ZnO morphologies via heating pure Zn under ambient conditions remains a challenge. In this report, we utilize a CuZn alloy (brass) to obtain CuO and ZnO nanostructures. By changing the Zn/Cu ratios in brass, the dominant products can be CuO nanowires, ZnO nanoflakes, and a mixture of both. Combining the effects of Cu in brass and the growth temperature, the morphology of ZnO can be 1D nanowires/nanoflakes, 2D nanosheets, or 3D networks with single-crystalline structures. The field emission (FE) properties of such a hybrid assembly of ZnO–CuO nanostructures from samples with different Zn concentrations are tested and compared.

Our results will shed light on the fabrication of nanohybrids via a simple and cost-effective way for their application in future multifunctional nanodevices. For example, ZnO nanostructures and thin films have been used as gas sensors to detect various kinds of vapors or gases, including ethanol,[5] O_2,[29] CO,[30] NH_3,[31] and H_2.[32] On the other hand, CuO nanowires have been studied as a gas-sensing device to detect CO, NO_2, and H_2S.[33] Sputtered CuO films also showed sensi-

[*] Prof. C.-H. Sow, Y. Zhu, P. Li
Department of Physics
National University of Singapore
2 Science Drive 3, 117542 (Singapore)
E-mail: physowch@nus.edu.sg
Prof. C.-H. Sow, Y. Zhu, Prof. J. T.-L. Thong
National University of Singapore
Nanoscience & Nanotechnology Initiative
S13, 2 Science Drive 3, 117542 (Singapore)
Dr. T. Yu, Prof. Z. Shen
School of Physical & Mathematical Sciences
Nanyang Technological University
1 Nanyang Walk, 637616 (Singapore)
Q. Zhao, Prof. D. Yu
School of Physics
Peking University
Beijing, 100871 (P.R. China)
Prof. J. T.-L. Thong
Department of Electrical and Computer Engineering
National University of Singapore
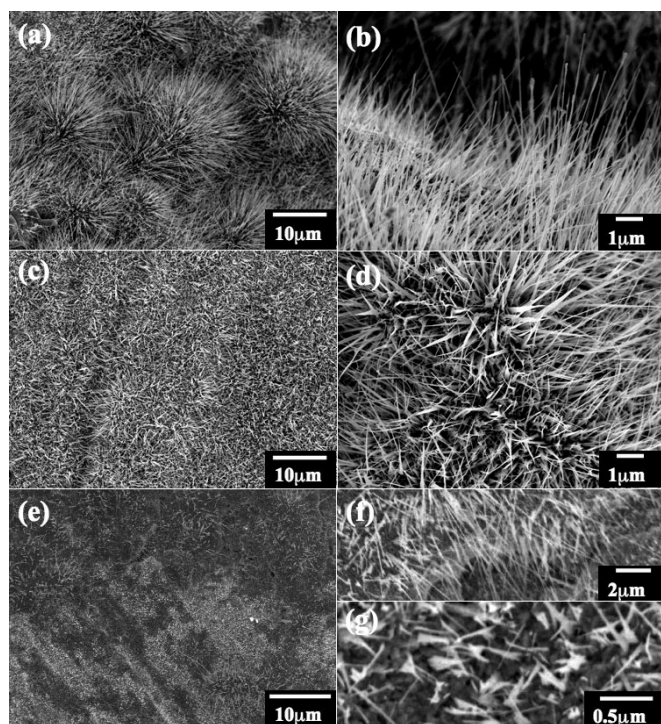4 Engineering Drive 3, 117576 (Singapore)

© 2006 WILEY-VCH Verlag GmbH & Co. KGaA, Weinheim

tivity to CO_2 and N_2.[34] Thus, a mixture of CuO nanowires and ZnO nanoflakes could provide a potentially useful multifunctional gas sensor. By changing their ratio in brass, selected sensitivity for a certain gas could be realized. In addition, the ZnO–CuO composite has been shown to be an effective catalyst with a high efficiency for eliminating some hazardous organic compounds such as phenol from waste water.[35] ZnO–CuO nanocomposites are expected to further enhance such performance with higher specific surface areas.

2. Results and Discussion

2.1. Growth and Characterizations of ZnO–CuO Nanostructures

At a growth temperature of 500 °C, the morphologies of products from different Zn contents were studied using scanning electron microscopy (SEM), with typical images shown in Figure 1. As we can see, both Zn 5 wt % (Fig. 1a and b) and Zn 40 wt % (Fig. 1c and d) samples were covered with a layer of uniform 1D nanostructures, which were locally aligned. From the Zn 5 wt % brass, the nanowires had an average length of 6–8 μm and a diameter of 40–60 nm. However, from the Zn 40 wt % sample flakelike nanostructures were observed with an average length of 4 μm and a very sharp tip of about 10–20 nm in diameter. The width of the nanoflakes gradually increased from the tip to the root, up to 100–200 nm. The aver-
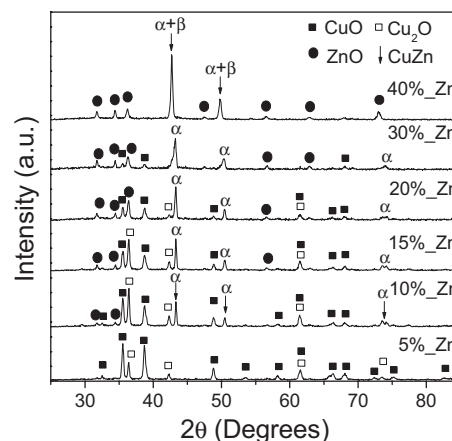
age thickness was about 10–20 nm. However, from Zn 15 wt % brass (Fig. 1e) the surface density of the nanostructures was much lower than those from Zn 5 wt % and Zn 40 wt % samples, even though the same growth temperature and duration were employed. Interlaced bright and dark regions were observed, which demonstrated similar nanowires (Fig. 1f) and nanoflakes (Fig. 1g), but with smaller lengths. Other samples with Zn concentrations between 5 and 40 wt % had morphologies similar to the Zn 15 wt % sample except that the area ratios of bright regions increased with increasing Zn concentrations. Figure 2 briefly summarizes the morphological dependence of products on the Zn concentrations in the brasses and growth temperatures.
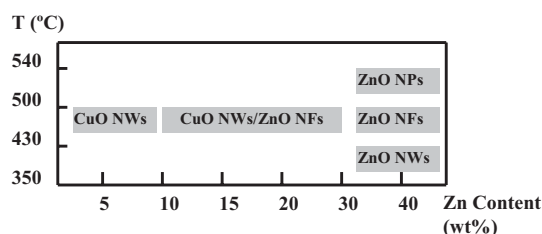
Figure 2. Morphological dependence of products on Zn contents in brass and growth temperatures. The following dominant morphologies are shown: CuO nanowires (CuO NWs), ZnO nanowires (ZnO NWs), ZnO nanoflakes (ZnO NFs) and ZnO nanopalms (ZnO NPs).

The structural phase evolution of the products with different Zn concentrations after heating at 500 °C was investigated by using X-ray diffraction (XRD). In Figure 3 we can see that, from Zn 5 wt % brass almost all remarkable peaks can be ascribed to the CuO structure. Several Cu_2O peaks were found and considered as the precursor for the growth of CuO nanowires.[36] With an increase in the Zn concentrations, the CuO/Cu_2O peaks gradually became weaker and finally disappeared for the Zn 40 wt % sample. On the other hand, ZnO structure began to appear from the Zn 10 wt % sample and dominated for the sample from Zn 40 wt % brass. For the sam-

Figure 1. Typical SEM images of the brass surface after heating at 500 °C in air for two days. a,b) Results from Zn 5 wt % brass at low and high magnifications, respectively. c,d) The products from Zn 40 wt % brass. e) A mixture of two morphologies from a Zn 15 wt % sample; the dark and bright regions in (e) are further enlarged in (f) and (g), repectively.
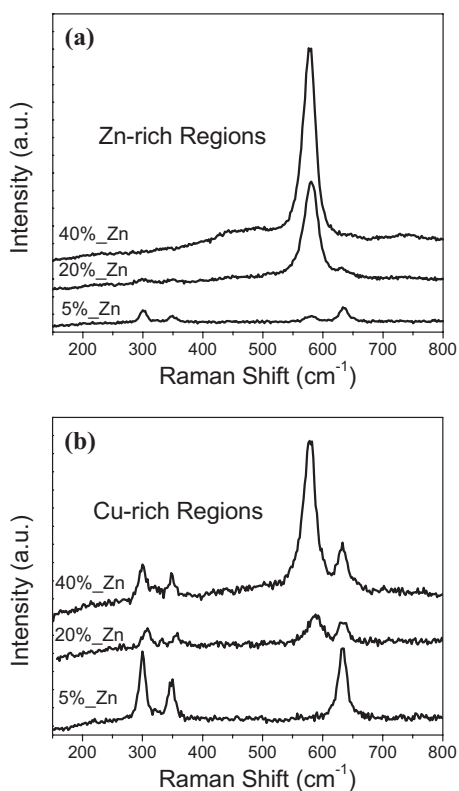

Figure 3. XRD spectra of the products with an increase in the Zn contents.

ples with Zn concentrations between 5 and 40 wt%, both products co-existed on one substrate simultaneously. Besides the ZnO and CuO peaks, it is worth noting that for the brasses with Zn concentration larger than 5 wt%, two peaks corresponding to the CuZn alloy phase were found.[37] It is known that an *α* phase is expected for a CuZn alloy with Zn content ranging from 0 to 38 wt%. This is followed by the duplex phase *α* + *β* and further *β* phase for an alloy with about 50 wt% Zn.[38–40] *α*-Brass shows a body-centered cubic (bcc) structure and *β*-brass a face-centered cubic (fcc) structure. Such a phase transition occurred when Zn content increased from 30 to 40 wt%, as shown in the XRD spectra.
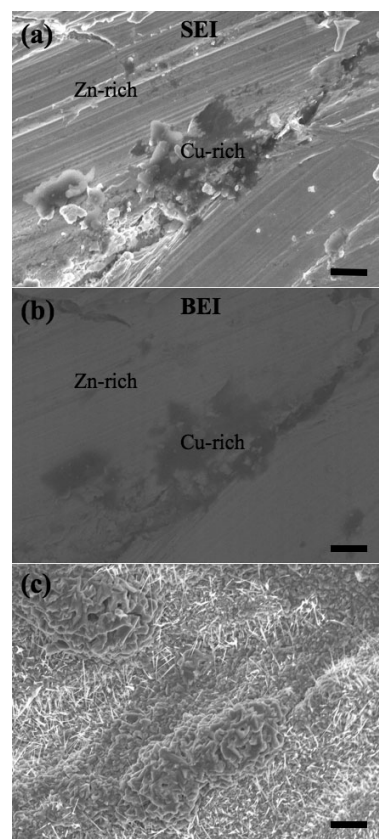
To further investigate the distribution of CuO and ZnO, micro-Raman spectroscopy was carried out and the spectra are shown in Figure 4. The peak located at 583 cm^{-1} corresponds to the E_1(LO) of ZnO,[41] and the three peaks at about 286, 335, and 625 cm^{-1} are attributed to the A_g, $B_g^{(1)}$, and $B_g^{(2)}$ modes of CuO due to the vibrations of oxygen atoms.[36] With an increase in the Zn concentration, the intensity of the ZnO peak increased and the intensity of CuO peaks decreased. From the spectra, we can see again that CuO and ZnO nanostructures grow from one brass substrate at the same time. However, the distribution of CuO and ZnO was not uniform and obviously different Raman signals were obtained from different regions. From the Zn-rich region (Fig. 4a), the ZnO E_1(LO) peak can be observed despite the fact that the sample contains only 5 wt% of Zn. In the Cu-rich region (Fig. 4b), for the sample with 40 wt% Zn, the peaks of CuO are still ob-

vious, but with intensities much lower than that of ZnO. Combining the results from SEM and XRD, it is obvious that ZnO was the dominant product of the synthesis, despite the fact that Zn content is lower than Cu. Moreover, the nonuniform mixture of Cu and Zn in brass resulted in separate but simultaneous growth of CuO nanowires and ZnO nanoflakes on one substrate, as shown in Figure 1e.

To investigate the effects of the distribution of Cu and Zn in brass more directly, the morphology of one region on Zn 15 wt% brass was compared before and after heating, as shown in Figure 5. Figure 5a and b shows the same region of the brass before heating with the scanning electron microscope operating in the secondary electron image (SEI) mode and the


Figure 5. Exactly the same region on Zn 15 wt% brass before (a) and after (c) heating in air. b) Backscattered electron image corresponding to the secondary electron image in (a). All scale bars are 1 μm.

backscattered electron image (BEI) mode, respectively. Although Zn and Cu have similar atomic weights, the contrast in the BEI is still suggestive of the difference between Zn-rich and Cu-rich regions. After heating at 500 °C for two days, it can be seen from Figure 5c that lots of short nanoflakes were grown from the Zn-rich region and very few nanowires were observed from the Cu-rich region, which was only sintered. Such results may be caused by the competition of Zn and Cu during the oxidization process. Obviously, the formation of ZnO is dominant due to the lower melting point and higher

Figure 4. Resonant micro-Raman spectra of different Zn contents in a) Zn-rich and b) Cu-rich regions.

vapor pressure of Zn than those of Cu under the same conditions. On the other hand, the existence of Cu in brass confined the growth of ZnO nanostructures. Such a role of Cu in brass may provide a natural way to control the position of ZnO nanostructure products.

Photoluminescence (PL) spectroscopy with a 325 nm laser focused on Zn-rich regions was used to further explore the effects of different Zn/Cu ratios. The spectra are shown in Figure 6. Two main peaks and one broad band were observed from the samples with Zn concentrations larger than 10 wt %.
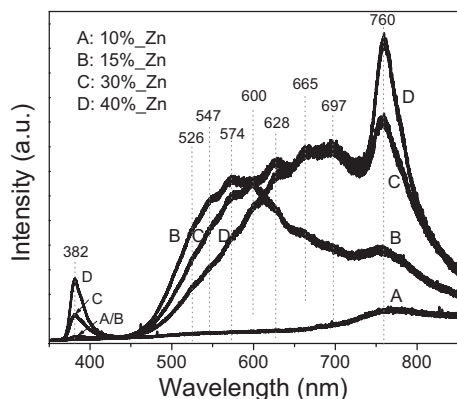

Figure 6. PL spectra of products varying with the Zn concentration in brass. All obvious peaks and shoulders are labeled with wavelength.

Since no significant PL signal was detected from CuO dominated samples, such strong PL is contributed to ZnO nanostructures. The PL of ZnO has been extensively studied for its potential optical applications.[41–44] All the peaks and remarkable shoulders composing the broad band were labeled to guide the eye. The UV peak at 382 nm (3.25 eV) is ascribed to the near-band-edge exciton recombination.[10,18,19,22,23] However, the broad band ranging from green to red is quite complicated due to the native and dopant-induced defects in ZnO, which are sensitively related to the synthesis procedures. Apart from the strong peak at 760 nm (1.63 eV), the visible band consists of at least another seven sub-peaks, resulting from the local levels in the bandgap of ZnO. The green shoulders at 526 nm (2.36 eV) and 547 nm (2.27 eV) are attributed to the antisite oxygen (O_{Zn}) and interstitial oxygen (O_i), respectively.[41,42] Two peaks at 600 nm (2.07 eV) and 628 nm (1.97 eV) are possibly caused by the monovalent vacancies of zinc (V_{Zn}^+) and oxygen (V_O^-) in ZnO.[41] The red peak at 665 nm (1.86 eV) is close to the band observed in a single ZnO nanowire and ZnO films,[43,44] which is also attributed to the single and double ionized oxygen vacancies. The strong peak at 760 nm

(1.63 eV) may be mainly caused by an oxygen vacancy (V_O),[42] since it is too strong to be ascribed to the second-order diffraction of UV emission.[44] The origin of another two peaks at 574 nm (2.16 eV) and 697 nm (1.78 eV) has been rarely mentioned and still unclear. It is worth noting that the feature of Cu-doping-induced green emission was not obvious in our case, although Cu ions are thought to be common factors to feature in the green emission in ZnO.[41,45–47] That is, Cu doping may not be significant in our ZnO nanostructures even though we fabricated them by heating CuZn alloys. Such a result could be related to the annealing process during synthesis. In addition, with an increase in the Zn content in brass, the UV and 760 nm peaks became stronger and the visible band shifted to longer wavelength, suggesting that with the increase of Zn content, the concentrations of oxygen vacancies in ZnO products become higher.

## 2.2. Morphological Control of ZnO Nanostructures

From the discussion above, we have seen that ZnO–CuO nanostructures can be synthesized simultaneously on one substrate by directly heating brasses with different Zn concentrations in air. Since characterizations have shown that the CuO nanowires were similar with those fabricated by heating a pure Cu plate,[24,36] and ZnO was the dominant product from the substrates with Zn concentrations higher than 20 wt %, we focus on the ZnO nanostructures in the following discussions. With the heating duration maintaining for two days, morphologies of ZnO from Zn 40 wt % brass were studied at different heating temperatures varying from 350 to 540 °C. Typical SEM images obtained are shown in Figure 7. At a temperature range between 350 and 430 °C, ZnO nanowires were obtained with
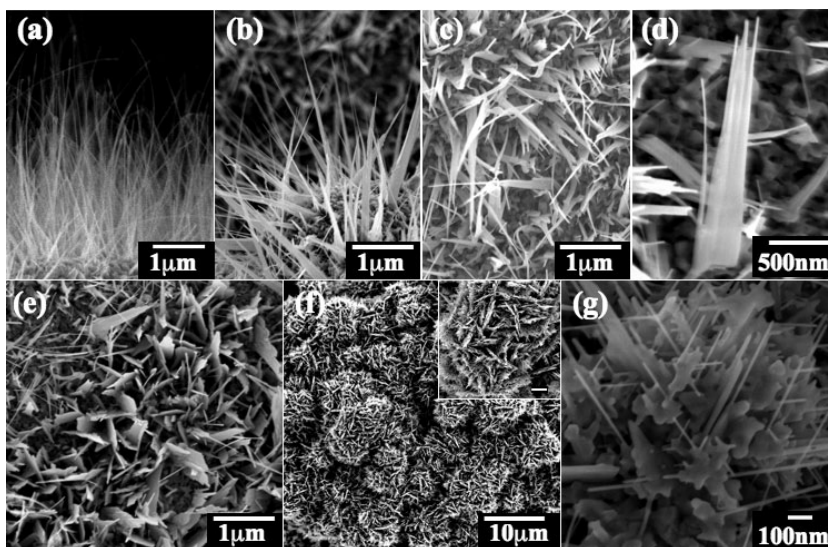
Figure 7. SEM images of ZnO nanostructures from Zn 40 wt % brass synthesized at different temperatures. a) Nanowires at 350–430 °C. b) Nanoflakes at 430–500 °C. c) Palmlike nanoflakes at 500–540 °C, and d) an individual branched nanoflake. e) ZnO nanosheets at 500–540 °C. f) ZnO microspheres; the inset highlights a sphere consisting of randomly distributed dendrites; the scale bar in the inset is 1 μm. g) High-magnification image of a ZnO network composed of nanowires and nanosheets with cubic assembly.

an average diameter of about 20 nm and an average length of 2–3 μm (Fig. 7a). When the temperature increased to 500 °C, nanoflakes were observed (Fig. 7b). For a growth temperature between 500 and 540 °C, massive palmlike or branched nanostructures were found from the substrate, as shown in Figure 7c. An individual ZnO nanopalm is further magnified in Figure 7d. The palm had a width of about 350 nm at the root part and separated into several nanowires with tip diameters of about 20 nm on the upper region. It is obvious that the contrast of the nanowires was different from that of the connection between them, possibly due to the different thickness. In addition, on some regions of the substrate, nanosheets were formed, which is shown in Figure 7e. Most nanosheets had rough edges and some of them also show palmlike morphology but with more nanotips, suggesting that the nanosheets may result from the subsequent lateral growth of the ZnO palms. More interestingly, after the brass was polished with sandpaper and cleaned in air before heating at 500–540 °C many microspheres were found near the edge of the substrate (Fig. 7f). These spheres had diameters ranging from 3 to 10 μm and piled together. Lots of branched dendrites were observed from the enlarged images (inset of Fig. 7f). In contrast to a previous report,[20] such dendrites did not lie in parallel planes, but distributed randomly and formed a sphere. A closer view into the dendrite (Fig. 7g) reveals a complicated 3D nanostructure of assembled nanowires and nanosheets. The 3D ZnO nanostructure is also different to the 2D dendrites[20] and other hierarchical structures[16,48] because there were no obvious main stems as starting points of the second growth and the angle between nanowires was nearly 90°. Such networks are similar to the results from cubic tungsten oxide nanostructures.[49] However, the typical ZnO network is only several hundred nanometers in size and the nanowires inside are typically 10–20 nm in diameter, much smaller than tungsten oxide networks reported by Zhou et al.[49]

Transmission electron microscopy (TEM) was used to investigate the microstructures of ZnO products from Zn 40 wt % brass after heating at 540 °C for two days. In Figure 8a it can be seen that many nanosheets were found, terminated with one or multiple nanowires. Most of the nanosheets were transparent, indicating a very small thickness. From a high-resolution TEM (HRTEM) image of a nanowire and the corresponding electron diffraction (ED) pattern (Fig. 8b and inset), we can clearly see the parallel fringes up to the surface of the nanowire. The fringe spacing was measured to be 0.28 nm, consistent with the {100} interplanar distance of wurtzite ZnO structure. The sixfold symmetric ED pattern verifies the single-crystalline structure and can be ascribed to the six faces equivalent to (100) of ZnO. The growth can be considered to be along the <110> direction, which is one of the fast-growth directions of ZnO and also consistent with previous reports.[20,23] Figure 8c shows a branched nanowire from a nanoflake, as we have seen in the palmlike structures above. The junction between the nanowire and the stem is highlighted (Fig. 8d) and further magnified in Figure 8e. It can be seen that the branch shared the same structure at the root part with the stem, but demonstrated {101} fringes. Figure 8f shows the HRTEM image of a nanosheet in
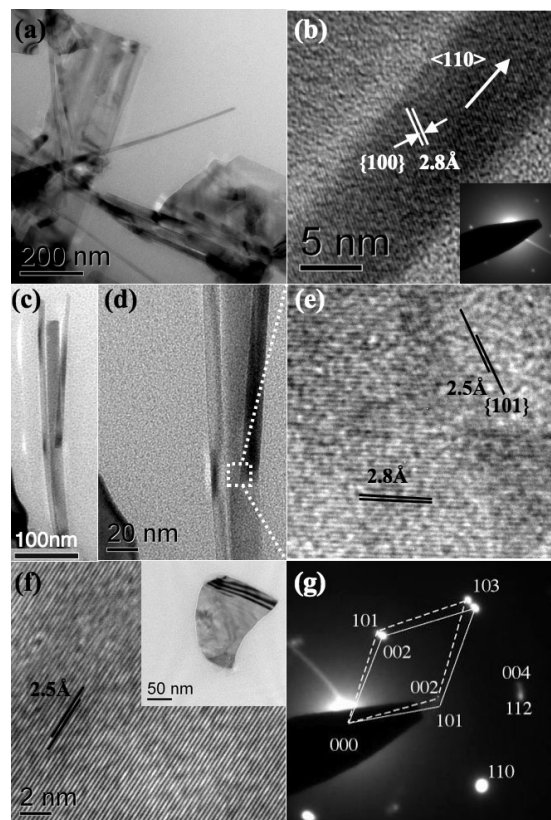
Figure 8. a) Typical TEM image of branched nanoflakes. b) High-resolution TEM (HRTEM) image of a nanowire, showing single-crystalline ZnO structure; the inset is the corresponding electron diffraction (ED) pattern with a crystal zone of <001>. c) A branched nanoflake with a highlight of the junction in (d); e) Crystalline fringes from the region in (d) marked with a square. f) HRTEM image of a nanosheet in the inset; the corresponding ED pattern is shown in (g), in which a twin structure with a zone of <010> can be indexed.
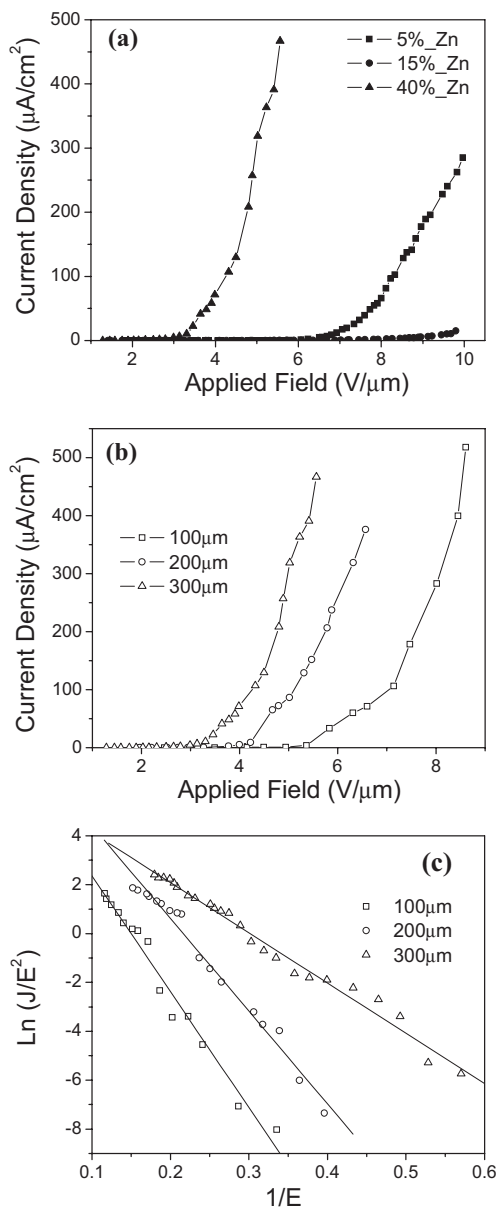
the inset. Once more, very clear crystal fringes were observed and the fringes are consistent with the interplanar spacing of {101} facets of ZnO. However, possibly due to the multiple layers of the nanosheet, the ED pattern revealed complicated features. This pattern is composed of at least two sets of single-crystal lattice, as indexed in Figure 8g. Obviously, a twin structure exists in the nanosheet, possibly because the nanosheet results from the extension or combination of close nanoflakes.[50]

From the results shown above, we can see that the morphology of the ZnO nanostructures is sensitive to the growth temperature and local Zn concentrations due to the nonuniform distribution of Zn in brass. Since the synthesis did not involve any catalyst and no particle terminators were found at the ends of the ZnO nanowires/nanoflakes, a normal vapor–liquid–solid mechanism is unlikely to be responsible for the growth of ZnO. Furthermore, as described above, higher temperature benefited the lateral growth and some nanoflakes demonstrated a bifurcated growth. These can be more reasonably explained by the "self-catalytic" nucleation,[20,21] and consequent tip-growth process.[23] When the temperature approaches the melting point of Zn (about 420 °C), Zn in brass would be melted into

liquid medium. Then the diffusion of oxygen could induce the oxidation of Zn. Since ZnO has a much higher melting point than Zn, it should readily solidify into solid particles and act as nuclei. The precipitation of ZnO clusters triggers the subsequent growth of 1D ZnO nanowires.[21] During the growth, Zn atoms could diffuse to the tip to sustain the growth.[23] Such a procedure is readily affected by the temperature. When the growth temperature increases, this would give rise to more rapid Zn diffusion and a higher supply of liquid Zn, resulting in longer nanoflakes and more-rapid lateral growth at the root part of the nanoflakes. The growth would slow down at a certain length due to the inefficient Zn supply to the tip. That is why the length of the ZnO nanoflakes is shown to saturate after four days of heating and also explains the very sharp tip of the nanoflakes. When the growth temperature continues to increase, merging of adjacent nanoflakes[50] or the presence of surface poisons or defects,[23] could be responsible for the branched structures and final palmlike 2D nanosheets. During the growth process, local Zn content in brass would further expedite or slow down the lateral growth. Due to the nonuniform mixture of Zn and Cu, more ZnO nanoflakes would be formed in some regions with higher local Zn concentrations and more 2D nanosheets would be formed. For some local regions with very high Zn concentrations, the oxidization process at high temperatures could be very fast and the growth along many directions may carry on at the same time, resulting in the complicated 3D ZnO networks. It is worth noticing that after heating pure Zn plates more 3D nanostructures and other complicated structures were obtained. Such a mechanism is also consistent with the results of other oxide nanostructures produced using similar methods.[25–27] Finally, the growth of ZnO from brass described above is closely related with the existence of Cu in brass. CuO nanowires have been fabricated at about 400 °C by heating pure Cu plates in air;[24] however, the growth of CuO 1D structures was suppressed by the formation of ZnO in this case. From the morphological changes of ZnO nanostructures with varying Zn (Cu) concentrations it appears that Cu acts as an impediment to the lateral growth of ZnO structures. On the micrometer scale, Figure 5 has clearly shown that the Zn/Cu interface in brass confined the coverage position and surface density of ZnO products. At a smaller scale, Cu clusters in brass may act as many tiny templates, confining the dimension of ZnO nanostructures on the brass surface. That is, the distribution of Cu in brass provides a natural way to control the formation of ZnO nanostructures. One of the metals in an alloy was seen to have a similar function in the synthesis of ion oxide nanowalls from FeMn films.[28]

2.3. FE from ZnO–CuO Nanostructures on Brass

The FE properties of our products on brasses after heating at 500 °C were measured under a 300 μm vacuum gap to check the effect of different Zn contents. Figure 9a compares the results from samples with 5, 15, and 40 wt % Zn concentrations, respectively. From Zn 5 wt % brass, in which CuO nanowires dominated, the turn-on field was about 6 V μm^{-1}. Here, we define the turn-on field as the field under which a current density is distinguished from the noise. Such a result is comparable to the previous report on CuO nanostructures from pure Cu,[51] but a little worse than our previous work.[24] For the sample with 40 wt % Zn content, the turn-on field significantly reduced to about 3 V μm^{-1} and a high current density of 470 μA cm^{-2} was obtained under a field of 5.5 V μm^{-1}, due to the excellent FE properties of ZnO nanowires/nanotips.[52–54] However, for the samples with medium Zn concentrations, for example, 15 wt % Zn, as shown in Figure 9a, only very low FE current was detected and the turn-on field increased to about 7–8 V μm^{-1}. The deteriorated FE could result from the super-

Figure 9. a) FE curves of brass samples with different Zn concentrations. b) FE of a Zn 40 wt % sample depending on vacuum gaps, and c) corresponding Fowler–Nordheim plots with linear fittings.

low surface density and much smaller length of the ZnO–CuO nanostructures, caused by the suppression of growth between CuO and ZnO, as shown in Figures 1e and 5. Other samples with Zn content between 5 and 40 wt % gave similar FE results. In addition, the effects of vacuum gap on the FE of ZnO nanoflakes from Zn 40 wt % brass were also studied and the results are shown in Figure 9b. We can see that with the reduction in the gap spacing *d*, the turn-on field gradually increased. Using the Fowler–Nordheim (FN) equation,[55] the enhancement factor (*γ*) can be estimated from the slope of the FN plots shown in Figure 9c. Taking the work function value of ZnO as 5.4 eV,[53,55] the *γ* value is about 1701 for *d* = 100 μm, 2127 for *d* = 200 μm, and 4065 for *d* = 300 μm. These values are much larger than those from ZnO nanopins[55] and TiSi$_2$ nanowires[56] measured under similar conditions in the same machine, which may be due to the sharper tips (about 10–20 nm) of our ZnO nanoflakes and rough-substrate-induced multistage effects,[57] caused by the cluster-shaped substrate underneath the ZnO nanoflakes, as shown in Figure 7b. Enhanced FE has been observed from ZnO nanowires grown on rough substrates such as carbon cloth.[3] On the other hand, a similar enhancement-factor dependence on the vacuum gap was recently reported for a single carbon nanotube (CNT),[58,59] and for nonplanar field emitters.[60] Silva and co-workers proposed that at low vacuum distance, the CNT emitter mimics a parallel-plate configuration and under far-field conditions the enhancement factor is no longer dependent on distance.[58] However, their far-field conditions (about 100 μm) were much smaller than that in our work. And the "two-region model" cannot explain our results, although it has satisfactorily explained the similar results from CNT arrays.[61] The mechanism for the vacuum-gap-dependent enhancement factors could be more complicated, deserving further investigation in our future work.

3. Conclusions

In summary, CuO–ZnO nanostructures have been synthesized by simply heating a CuZn alloy with different Zn concentrations in air. It was shown that with an increase in the Zn content the main products transitioned from CuO nanowires to ZnO nanoflakes. The suppression of CuO and ZnO was observed for the brasses with medium Zn contents. Depending on the growth temperature and local Zn content, the ZnO could be 1D nanowires/nanoflakes, 2D nanosheets, and 3D networks. Electron microscopy revealed the single-crystalline nature of ZnO nanoflakes and nanosheets. A tip-growth mechanism was proposed to explain the formation of different ZnO nanostructures with the help of Cu in brass. Excellent FE property was obtained from the Zn 40 wt % sample, which showed large enhancement factors with the values depending on the vacuum gaps. Such a composite nanostructure system may help to integrate the functions of both materials onto one device. It is also expected that this method can be expanded to other alloy systems to produce hybrid nanomaterials or to control the morphology of products by the component ratios in the alloy.

4. Experimental

To synthesize ZnO–CuO nanostructures, a piece of brass with a typical dimension of 10 mm × 10 mm (Super Conductor Materials, 1 mm thick, 99.9 %) was heated on a hot plate in air for two days. The concentration of Zn in brass varied from 5 wt to 40 wt %. After heating, the low-Zn-content samples became black and the high ones showed a grey–white color. The heating temperature varied between 350 and 540 °C in order to synthesize ZnO with different ZnO morphologies. After cooling down, the surface layer of products were characterized and analyzed using SEM (JEOL JSM-6400F), XRD (Bruker Analytical X-Ray System, Cu Kα radiation, *λ* = 1.5406 Å), micro-Raman/PL spectroscopy (Renishaw, 325 nm, 40 mW), and TEM (JEOL JEM-3010, 300 kV). FE measurements were carried out by a two-parallel-plate configuration in a vacuum chamber with a pressure of 3×10^{-7} Pa. The samples on brass substrates were attached to a stainless-steel plate using conducting glue as a cathode with the other stainless-steel plate as an anode. The distance between the electrodes was adjusted by a fine screw with a resolution of 10 μm. All samples were first heated for 15 min to degas and to further improve the vacuum. The emission current was monitored using a Keithley 485 picoampermeter.

[1] *Nanowires and Nanobelts—Materials, Properties and Devices* (Ed: Z. L. Wang), Kluwer, Dordrecht, The Netherlands **2003**.

[2] M. H. Huang, S. Mao, H. Feick, H. Q. Yan, X. Y. Wu, H. Kind, E. Weber, R. Russo, P. D. Yang, *Science* **2001**, *292*.

[3] D. Banerjee, S. H. Jo, Z. F. Ren, *Adv. Mater.* **2004**, *16*, 2028.

[4] H. Zhang, D. Yang, X. Ma, D. Que, *J. Phys. Chem. B* **2005**, *109*, 17 055.

[5] Q. Wan, Q. H. Li, Y. J. Chen, T. H. Wang, X. L. He, J. P. Li, C. L. Lin, *Appl. Phys. Lett.* **2004**, *84*, 3654.

[6] J. L. Yang, S. J. An, W. I. Park, G. C. Yi, W. Choi, *Adv. Mater.* **2004**, *16*, 1661.

[7] E. Hosono, S. Fujihara, I. Honma, H. Zhou, *Adv. Mater.* **2005**, *17*, 2091.

[8] Q. Wan, C. L. Lin, X. B. Yu, T. H. Wang, *Appl. Phys. Lett.* **2004**, *84*, 124.

[9] H. T. Ng, J. Han, T. Yamada, P. Nguyen, Y. P. Chen, M. Meyyappan, *Nano Lett.* **2004**, *4*, 1247.

[10] J. Q. Hu, Y. Bando, *Appl. Phys. Lett.* **2003**, *82*, 1401.

[11] Z. W. Pan, Z. R. Dai, Z. L. Wang, *Science* **2001**, *291*, 1947.

[12] X. Y. Kong, Y. Ding, R. Yang, Z. L. Wang, *Science* **2004**, *303*, 1348.

[13] P. Q. Yan, R. R. He, J. Johnson, M. Law, R. J. Saykally, P. D. Yang, *J. Am. Chem. Soc.* **2003**, *125*, 4728.

[14] H. T. Ng, J. Li, M. K. Smith, P. Nguyen, A. Cassell, J. Han, M. Meyyappan, *Science* **2003**, *300*, 1249.

[15] P. Q. Yan, R. R. He, J. Pham, P. D. Yang, *Adv. Mater.* **2003**, *15*, 402.

[16] J. Y. Lao, J. G. Wen, Z. F. Ren, *Nano Lett.* **2002**, *2*, 1287.

[17] Z. R. Tian, J. A. Voigt, J. Liu, B. Mckenzie, M. J. Mcdermott, M. A. Rodriguez, H. Konishi, H. N. M. Xu, *Nat. Mater.* **2003**, *2*, 821.

[18] J. Jie, G. Wang, Q. Wang, Y. Chen, X. Han, X. Wang, J. G. Hou, *J. Phys. Chem. B* **2004**, *108*, 11 976.

[19] Y. F. Zhang, R. E. Russo, S. S. Mao, *Appl. Phys. Lett.* **2005**, *87*, 133 115.

[20] H. J. Fan, R. Scholz, F. M. Kolb, M. Zacharias, *Appl. Phys. Lett.* **2004**, *85*, 4142.

[21] H. Y. Dang, J. Wang, S. S. Fan, *Nanotechnology* **2003**, *14*, 738.

[22] Q. Yang, K. Tang, J. Zuo, Y. Qian, *Appl. Phys. A* **2004**, *79*, 1847.

[23] X. Wen, Y. Fang, Q. Pang, C. Yang, J. Wang, K. Ge, K. S. Wong, S. J. Yang, *J. Phys. Chem. B* **2005**, *109*, 15 303.

[24] Y. W. Zhu, T. Yu, F. C. Cheong, X. J. Xu, C. T. Lim, V. B. C. Tan, J. T. L. Thong, C. H. Sow, *Nanotechnology* **2005**, *16*, 88.

[25] T. Yu, Y. Zhu, X. Xu, Z. Shen, P. Chen, C. T. Lim, J. T. L. Thong, C. H. Sow, *Adv. Mater.* **2005**, *17*, 1595.

[26] Y. W. Zhu, T. Yu, C. H. Sow, Y. J. Liu, A. T. S. Wee, X. J. Xu, C. T. Lim, J. T. L. Thong, *Appl. Phys. Lett.* **2005**, *87*, 023 103.

[27] T. Yu, Y. Zhu, X. Xu, K. S. Yeong, Z. Shen, P. Chen, C. T. Lim, J. T. L. Thong, C. H. Sow, *Small* **2006**, *2*, 80.

[28] B. Zong, Y. Wu, G. Han, B. Yang, P. Luo, L. Wang, J. Qiu, K. Li, *Chem. Mater.* **2005**, *17*, 1515.

[29] M.-C. Jeong, B. Y. Oh, O.-H. Nam, T. Kim, J.-M. Myoung, *Nanotechnology* **2006**, *17*, 526.

[30] H.-W. Ryu, B.-S. Park, S. A. Akbar, W.-S. Lee, K.-J. Hong, Y.-J. Seo, D.-C. Shin, J.-S. Park, G.-P. Choi, *Sens. Actuators B* **2003**, *96*, 717.

[31] G. Sberveglieri, *Sens. Actuators B* **1995**, *23*, 103.

[32] X. L. Cheng, H. Zhao, L. H. Huo, S. Gao, J. G. Zhao, *Sens. Actuators B* **2004**, *102*, 248.

[33] K. Sawicka, M. Karadge, A. K. Prasad, P. I. Gouma, *Microsc. Microanal.* **2004**, *10*, 360.

[34] P. Samarasekara, N. T. R. N. Kumara, N. U. S. Yapa, *J. Phys. Condens. Matter* **2006**, *18*, 2417.

[35] A. Fortuny, C. Bengoa, J. Font, A. Fabregat, *J. Hazardous Mater. B* **1999**, *64*, 181.

[36] T. Yu, X. Zhao, Z. X. Shen, Y. H. Wu, W. H. Su, *J. Cryst. Growth* **2004**, *268*, 590.

[37] Joint Committee on Powder Diffraction Standards card number 25-0322, **2000**.

[38] T. B. Massalski, H. Okamoto, P. R. Subramanian, L. Kacprzak, *Binary Alloy Phase Diagrams*, American Society for Metals, Materials Park, OH **1990**.

[39] Y. Zhou, W. Zhang, J. Guo, G. He, *Philos. Mag. Lett.* **2004**, *84*, 341.

[40] D. F. Rendle, *Rigaku J.* **2003**, *20*, 11.

[41] C. X. Xu, X. W. Sun, X. H. Zhang, L. Ke, S. J. Chua, *Nanotechnology* **2004**, *15*, 856.

[42] B. Lin, Z. Fu, Y. Jia, *Appl. Phys. Lett.* **2001**, *79*, 943.

[43] Z. Fan, P. C. Chang, J. G. Lu, E. C. Walter, R. M. Penner, C. H. Lin, H. P. Lee, *Appl. Phys. Lett.* **2004**, *85*, 6128.

[44] Y. G. Wang, S. P. Lau, H. W. Lee, S. F. Yu, B. K. Tay, X. H. Zhang, H. H. Hng, *J. Appl. Phys.* **2003**, *94*, 354.

[45] N. Y. Garces, L. Wang, L. Bai, N. C. Giles, L. E. Halliburton, G. Cantwell, *Appl. Phys. Lett.* **2002**, *81*, 622.

[46] R. Dingle, *Phys. Rev. Lett.* **1969**, *23*, 579.

[47] S. M. Zhou, X. H. Zhang, X. M. Meng, K. Zou, X. Fan, S. K. Wu, S. T. Lee, *Nanotechnology* **2004**, *15*, 1152.

[48] P. Gao, Z. L. Wang, *J. Phys. Chem. B* **2002**, *106*, 12 653.

[49] J. Zhou, Y. Ding, D. S. Z., L. Gong, N. S. Xu, Z. L. Wang, *Adv. Mater.* **2005**, *17*, 2107.

[50] J. H. Park, H. J. Choi, J. G. J. Park, *J. Cryst. Growth* **2004**, *263*, 237.

[51] C. T. Hsieh, J. M. Chen, H. H. Lin, H. C. Shih, *Appl. Phys. Lett.* **2003**, *83*, 3383.

[52] C. X. Xu, X. W. Sun, *Appl. Phys. Lett.* **2003**, *83*, 3806.

[53] Y. W. Zhu, H. Z. Zhang, X. C. Sun, S. Q. Feng, J. Xu, Q. Zhao, B. Xiang, R. M. Wang, D. P. Yu, *Appl. Phys. Lett.* **2003**, *83*, 144.

[54] J. B. Cui, C. P. Daghlian, U. J. Gibson, R. Püsche, P. Geithner, L. Ley, *J. Appl. Phys.* **2005**, *97*, 044 315.

[55] Q. H. Li, Q. Wan, Y. J. Chen, T. H. Wang, H. B. Jia, D. P. Yu, *Appl. Phys. Lett.* **2004**, *85*, 636.

[56] B. Xiang, Q. X. Wang, Z. Wang, X. Z. Zhang, L. Q. Liu, J. Xu, D. P. Yu, *Appl. Phys. Lett.* **2005**, *86*, 243 103.

[57] J. Y. Huang, K. Kemp, S. H. Jo, S. Chen, Z. F. Ren, *Appl. Phys. Lett.* **2005**, *87*, 053 110.

[58] R. C. Smith, D. C. Cox, S. R. P. Silva, *Appl. Phys. Lett.* **2005**, *87*, 103 112.

[59] Z. Xu, X. D. Bai, E. G. Wang, *Appl. Phys. Lett.* **2006**, *88*, 133 107.

[60] R. C. Smith, R. D. Forrest, J. D. Carey, W. K. Hsu, S. R. P. Silva, *Appl. Phys. Lett.* **2005**, *87*, 013 111.

[61] D. Y. Zhong, G. Y. Zhang, S. Liu, T. Sakurai, E. G. Wang, *Appl. Phys. Lett.* **2002**, *80*, 506.

———————————————